

A Compliant Underactuated Hand with Suction Flow for Underwater Mobile Manipulation

Hannah S. Stuart, Shiquan Wang, Bayard Gardineer, David L. Christensen, Daniel M. Aukes, Mark Cutkosky
 Center for Design Research – Stanford University – Stanford, CA 94305-2232, USA

Abstract— Fingertip suction is investigated using a compliant, underactuated, tendon-driven hand designed for underwater mobile manipulation. Tendon routing and joint stiffnesses are designed to provide ease of closure while maintaining finger rigidity, allowing the hand to pinch small objects, as well as secure large objects, without diminishing strength. While the hand is designed to grasp a range of objects, the addition of light suction flow to the fingertips is especially effective for small, low-friction (slippery) objects. Numerical simulations confirm that changing suction parameters can increase the object acquisition region, providing guidelines for future versions of the hand.

I. INTRODUCTION

Diving is a dangerous occupation. Not only are divers susceptible to drowning, hypothermia, and decompression sickness but these risks are exacerbated by strenuous work, extended dive length, and dive frequency. Occupational divers may be expected to direct large machinery and handle power tools, such as underwater cutters and welders, which heighten the risk. The U.S. Bureau of Labor Statistics recorded in 2011 that divers were subject to 38 times the average national occupational death rate (about 3.5 in 100,000)¹. An underwater humanoid robot could potentially perform many of the manual tasks that human divers perform today while providing an intuitive platform for remote operation.

The application for the hand described in this paper is a new underwater robot intended for exploration and biological research in coral reef zones in the Red Sea. The robot, which is being developed through a collaboration between the King Abdullah University of Science and Technology (KAUST) Red Sea Research Center², Meka Robotics³, and Stanford University, will allow marine biologists to remain above water while obtaining specimens, positioning equipment, and performing other monitoring and maintenance tasks down to 100 m below the surface, at pressures up to 11 bar.

As in other examples of mobile manipulation, it is desirable for hands to be robust and compliant. The hand should also be low-mass because it will contribute disproportionately to the arm inertia and is the most frequent site of contact (intentional and accidental) with the environment. Accordingly, the hand is compliant, underactuated, and backdrivable and uses flexures instead of pin joints, subsequently reducing mechanical complexity. In this regard, it shares similarities with other compliant hands designed for mobile manipulation including [1]–[8]. The particular requirement

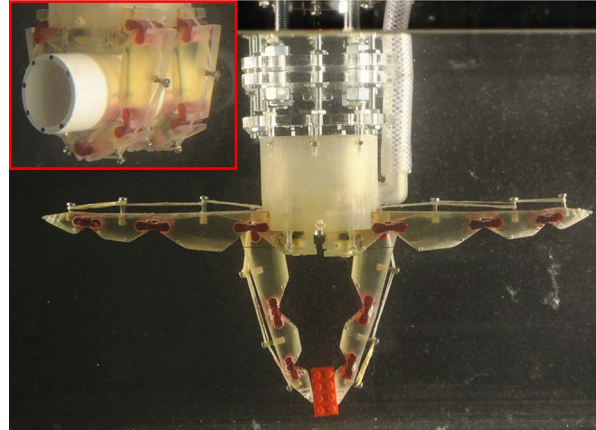


Fig. 1: Examples of the hand prototype grasping a small object (below) and a large tube (inset) underwater.

of grasping small, delicate and slippery objects has led to the incorporation of a gentle suction flow at the fingertips to enhance the region of object acquisition in water.

In the following sections, we describe the grasping requirements that govern the design of the hand, including the number and orientation of fingers, joint stiffnesses, and tendon routing schemes. Given the large space of configurations and parameters, it is infeasible to perform a global optimization. In addition to force and compliance analyses, fast dynamic simulations are useful for rapidly evaluating different hand designs as they interact with objects underwater. We briefly describe the analysis approach, which is adapted from [9], including a new model of fingertip suction that enlarges the acquisition region. We next describe suction experiments conducted in water and conclude with a discussion of lessons learned for the next iteration of this underwater hand.

II. GRASPING AND MANIPULATION REQUIREMENTS

This project specifies that the robot must be able to perform certain tasks: sample delicate live specimens, like deep-sea sponges; collect coral samples using a chisel and hammer; deploy and position long-term sensing equipment or structures; retrieve samples below overhangs and in crevices; and, operate tools designed for human divers. Therefore, this hand must be able to perform enveloping, secure grasps as well as precision, sensitive pinch grasps (which are inherently less stable). Using established grasp taxonomies [10,11], the essential grasp types can be identified to meet the remote manipulation needs. A large diameter and small diameter heavy wrap, as well as a medium prismatic wrap,

¹<http://www.bls.gov/iif/oshcfo11.htm>

²<http://rsrc.kaust.edu.sa>

³<http://mekabot.com>

can achieve many of the equipment grasping requirements on, for example, chisels, pipes and cutting tools. A delicate two-fingered pinch can account for soft, slippery organic sample handling. The versatility of these grasps provides a range of stability or sensitivity to choose from when manipulating objects of various shape and surface friction.

III. HAND AND FINGER DESIGN

The requirements of achieving both wrap and pinch grasps on large and small objects in a highly unstructured environment have led to the choice of a hand with four fingers, each driven by a single actuator. While a three-fingered hand could achieve most of the desired grasp types, it would have less stability when handling long cylindrical objects. The two pairs of compliant opposed fingers are slightly offset so that, in addition to pinching small objects (Fig. 1), they can bend laterally and slide past each other under large grasp forces to produce an interlaced grasp (Fig. 1(inset) and Fig. 2(right)). This solution is simpler and easier to waterproof than a reconfigurable palm, as used in some other hands [9]. One drawback with fixed fingers is the inability to perform as many in-hand manipulations. The current finger locations also allow small objects to escape from a wrap grasp.

A. Tendon routing and return springs

A critical requirement in the design of underactuated fingers is to obtain the right balance, at each configuration, of joint torques due to the tendon and the passive stiffness elements. A known concern is to prevent premature curling of the fingers, which makes it difficult to grasp small objects in a pinch grasp. Solutions can include actuating the finger with linkages, modifying the effective transmission ratios of the cables, using variable stiffness springs, or using

secondary cables in the finger mechanism [12]–[15]. In the present case, a simple, water-resistant solution is desired.

The finger stiffness at each joint is determined by a combination of the elastomeric flexure and an external extension spring, implemented with elastic bands in the prototype, as shown in Fig. 3. In general, for stability and resistance to external forces, the proximal joints should be stiff. However, this can lead to premature curling of the distal joints as the hand closes, unless the distal joints are even stiffer. As joint stiffnesses are increased, the ability of the hand to apply large grasp forces is reduced because the actuators continually work against the hand's own springs. To overcome these effects and decrease flexure stiffness, there is a second set of extension springs on the back side of each finger.

In addition, the tendon does not wrap around a pulley at the joint and, instead, acts upon the joint flexure with a variable geometry. This is accomplished with polished stainless steel dowel pins which are installed at each entry and exit location of the tendon on each phalanx, as well as at all tendon direction changes in the base of the finger. This reduces friction and tendon wear considerably as compared to rubbing against the bare 3D printed material. As the hand closes, the effective lever arm of the tendon increases along with mechanical advantage and grasp force capabilities. The tendon terminates at a pulley in the base of the finger which is driven by a motor on the other side of a shaft seal. This modular design allows the finger to be removed or broken without compromising the waterproof seal of the palm.

Figure 4 shows a simplified model with lumped-parameter stiffness elements that can be used to determine relative stiffnesses and dimensions of a joint. Because the flexures are short and soft compared to the phalanges, it suffices to approximate them at this stage with pin joints, although more accurate models are available [16]. Using vision and markers, we experimentally verified that the proximal phalanx's center of rotation is approximately fixed throughout the range of motion of interest, similar to [3]. The termination points of the tendon and extension springs are also assumed to be constant although there are small variations due to rolling contact and compliance.

The moment arms, or effective radii, of the tendon (\vec{R}_f) and extension spring (\vec{R}_e) are defined as the position vectors

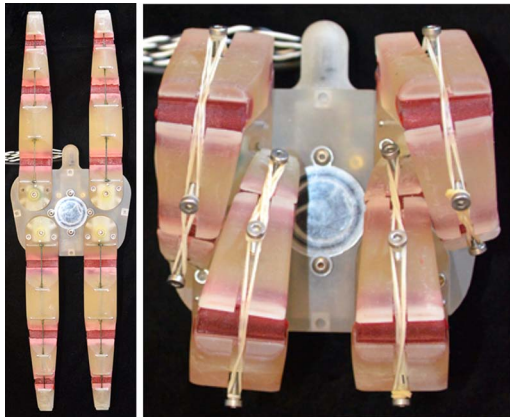


Fig. 2: Palm layout (left). The flexures can twist allowing the fingers to interlace for a wrap grasp (right).

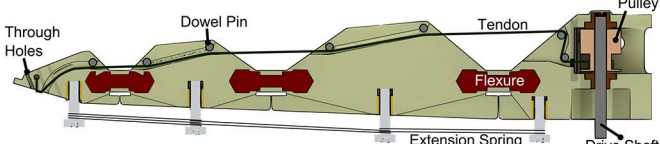


Fig. 3: Finger cross section, tendon routing, and finger hardware details.

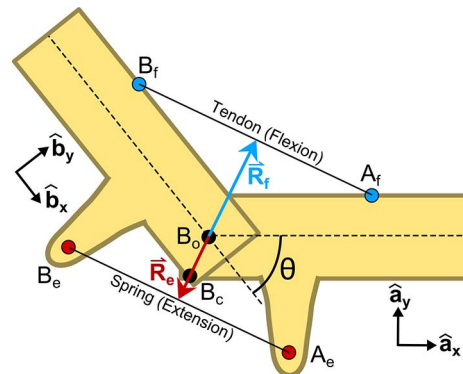


Fig. 4: Simplified joint model using lumped-parameter stiffness elements.

perpendicular to the tendon or spring from B_o , such that:

$$R_f = \left| \vec{R}_f \right| = \left| \vec{r}^{B_o/B_f} \times \frac{\vec{r}^{A_f/B_f}}{\left| \vec{r}^{A_f/B_f} \right|} \right| \quad (1)$$

$$R_e = \left| \vec{R}_e \right| = \left| \vec{r}^{B_o/B_e} \times \frac{\vec{r}^{A_e/B_e}}{\left| \vec{r}^{A_e/B_e} \right|} \right| \quad (2)$$

with the notation defined such that $\vec{r}^{A/B}$ is the position vector to point A from point B .

The stretch S is the distance between A_e and B_e minus the natural length of the spring s_n until the spring makes contact with the flexure, in which case a point contact is assumed at B_c , where $\vec{r}^{B_c/B_o} = \frac{1}{2}h \frac{\vec{R}_e}{\left| \vec{R}_e \right|}$

$$S = \begin{cases} \left| \vec{r}^{A_e/B_e} \right| - s_n, & \left| \vec{R}_e \right| > \frac{1}{2}h \\ \left| \vec{r}^{A_e/B_c} \right| + \left| \vec{r}^{B_e/B_c} \right| - s_n, & \left| \vec{R}_e \right| \leq \frac{1}{2}h. \end{cases} \quad (3)$$

After solving these trigonometric equations using Motion-Genesis™, it is straightforward to calculate the moments applied to each joint by the flexure, extension spring, and tendon given any angle:

$$\vec{M}^{B/B_0} = \left[\left| \vec{R}_e \right| k_{spring} S - \left| \vec{R}_f \right| T \right] \hat{a}_z \quad (4)$$

where k_{spring} is the stiffness of the extension spring and T is the magnitude of the tendon tension force.

As seen in Fig. 1, the varying extension spring and tendon effective radii allow for pinching small objects and wrapping around large objects. As demonstrated in Fig. 5, with variable R_e and R_f , there is a moderate initial tendon force to prevent sagging due to gravity, buoyancy, or strong water flow in the open position, without requiring a large tendon force to overcome the finger stiffness when the finger is curled.

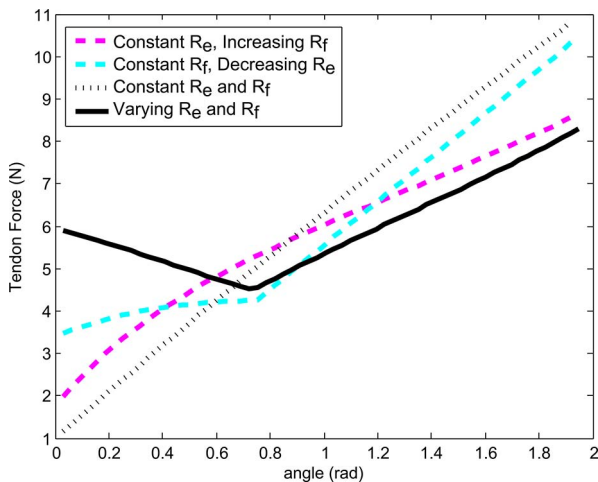


Fig. 5: Tendon tension required to hold the middle joint in static equilibrium over its range of joint angles. This comparison was conducted using the measured average stiffness of the middle joint. Constant radii equivalents were calculated by averaging the radii of the nonlinear case over the range of angular displacement.

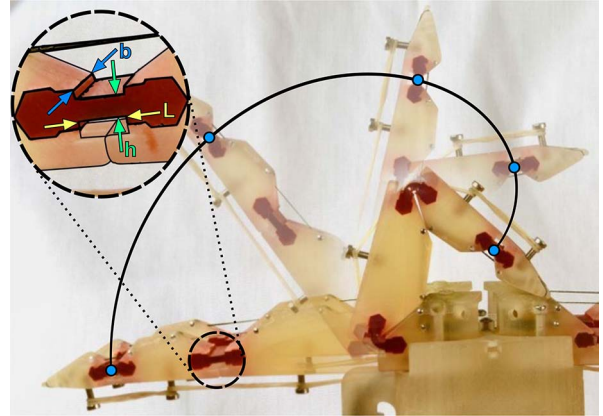


Fig. 6: Detail of the joint flexures with dimensions (top left). Demonstration of finger curl, from proximal to distal (main).

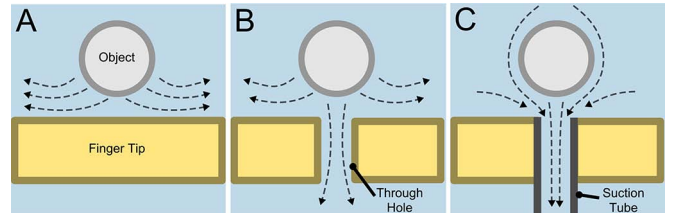


Fig. 7: (A) Water flowing away from the object-hand interface during grasping can push the object away, reducing grasp success. (B) Through holes can alleviate the effects of the instability demonstrated in (A). (C) If suction flow is applied to the finger hole, a stable position for the object is created at the finger surface to improve grasp success.

B. Flexure Design

Simplified rotational stiffness for the urethane flexure joints is characterized using large-deflection analysis for a beam with a moment end load [17].

$$k_{flex} = \frac{M}{\theta} = \frac{EI}{L} \quad (5)$$

where the I is the moment of inertia, M is the moment applied to the free end of a cantilevered beam, θ is the angle of the end of the beam with respect to the base, L is the arc length of the beam, and E is the Young's modulus. Flexure stiffness is therefore a function of the geometry detailed in Fig. 6. Although E is not constant with large deflection, we experimentally verified that flexure stiffness is approximately constant for this specific design. More detailed material modeling of the flexure will be a part of future work.

C. Suction System

Underwater grasping provides additional challenges as compared to manipulation in air. Not only does object buoyancy become a significant factor in grasping, but as the finger approaches the object fluid interactions tend to push the object away, making grasping more difficult (Fig. 7). Mitigating or reversing this interaction can improve grasping, especially for light, small objects. For example, oceanic feeding fish employ local suction flow to catch mobile prey [18,19]. Accordingly, a slight suction flow was built into the fingertips to assist the fingers in acquiring and pinching

delicate or slippery objects. Suction is applied to through-holes from the back side of the finger, with tubing running up the hand to an external pump. The flow rate is kept relatively low, to prevent disturbing the local environment or acquiring undesired objects in the vicinity. An additional membrane may prevent aspirating dirt or silt. In comparison to suckers [20], this suction flow does not rely on forming a seal.

D. Fabrication

The hand prototype was fabricated using a combination of 3D printing and casting similar to the approach used for [6,21]. The fingers were printed using a Projet 3500 3D Printer out of Visijet Crystal. The flexure molds were printed between the phalanges to make each finger one continuous piece. The dog-bone shaped flexures (Figs. 3 & 6) were then cast in urethane (Smooth-on PMC 780, with Young's modulus of approximately 2.76 MPa). Stress-concentrating grooves were included around the mold walls such that they would easily break away, leaving a smooth joint flexure.

IV. MODELING AND SIMULATION

While analytic models can be used to explore the mapping from actuator effort to grasp forces and to evaluate grasp quality, they must be reformulated whenever contacts are made or broken, which can happen with any change in the variables that govern how the fingers close upon an object. A dynamic simulation package can be useful for evaluating hand designs and should be designed to detect and respond efficiently to changes in contact conditions and friction. As in [5,9], the simulation presented here is based on Moby [22]. In the present application, in addition to the masses, object buoyancy, tendon forces, joint stiffnesses, and friction, suction must be accounted for as well. The general fluid dynamics are too complex for inclusion, but a simplified

model of the effects of drag and suction is necessary since such forces influence object behavior near the fingertips.

The simulation structure is shown in Figure 8. The object controller calculates the forces, including any drag or suction forces, on the object for each computing cycle, based on the object's position and velocity. The hand controller computes the forces on the fingers due to the tendons, flexure stiffnesses, and contacts. The effects of suction and drag are not computed for the fingers as they are negligible compared to the tendon and contact forces. At each computing cycle, the simulation checks whether the center of mass of the object is contained within a polygon formed by the joints of the fingers as shown in Figure 9. This is a quick test of whether the object has escaped or been grasped (as opposed to waiting for the simulation to settle to equilibrium with every run) and speeds up computation time. A simplified version of the configuration-dependent mapping from tendon and extension spring force to joint torque, as described in Section III(A), is obtained by fitting a second-order polynomial to the kinematic relationships obtained for the given geometry.

A. Drag and suction computations

When a submerged object, such as a cylinder, moves with a moderate speed (Reynolds number > 1000), the drag force increases approximately with the square of velocity [23]:

$$F_d = \frac{1}{2} \rho v^2 C_d A \quad (6)$$

where ρ is the fluid density, v is the speed of object relative to the fluid, A is the cross-sectional area of the object towards the flow and C_d is the drag coefficient. At low speeds, the drag is viscous:

$$F_d = F_D \mu v h \quad (7)$$

where F_D is the non-dimensional drag. The coefficients C_d and F_D are obtained empirically as 0.47 and 37.33 [24].

When an object approaches a fingertip, it experiences an additional force due to the suction mechanism described in Section III-C. The details of the suction effect depend on the geometry of the fingertip and object, and are complex. However, a useful approximation can be obtained for the case when the distance between the two surfaces is small as compared to their radii of curvature. Flow is modeled as an inlet pipe attached to one of two parallel plates (Fig. 10). Conservation of flow implies that

$$v(r) = \frac{Q}{2\pi r \delta} \quad (8)$$

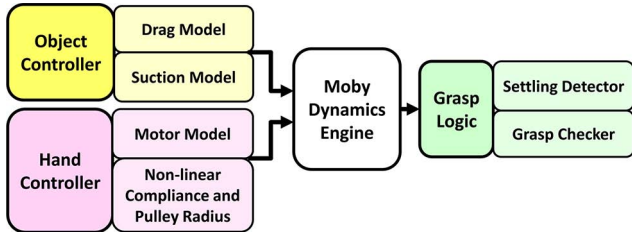


Fig. 8: Simulator structure.

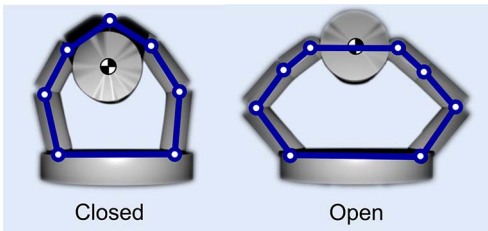


Fig. 9: Simulation rendering displaying the relative positions of the object's center of mass and the polygon of connected joint vertices in the case of a closed/successful (left) and open (right) grasp. In the closed case, simulation speed can be accelerated by assuming grasp success. In the open case, this assumption is abandoned and the simulator must wait until the finger and object settle.

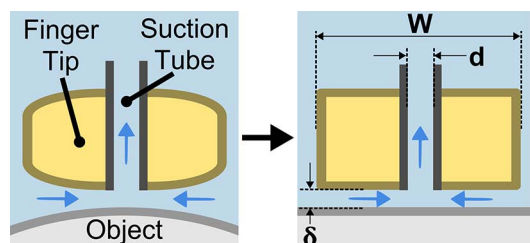


Fig. 10: General (left) and simplified (right) 2D suction model.

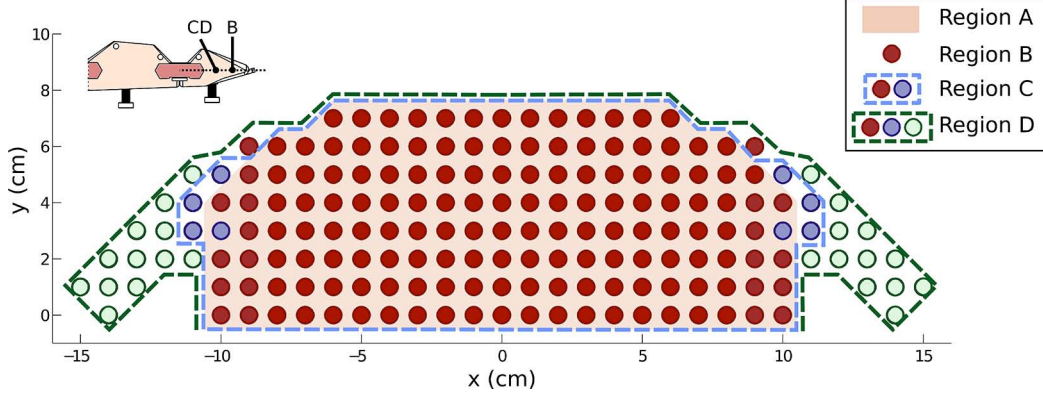


Fig. 11: Simulated grasp region with suction. (Region A: grasp without suction. Region B: grasp with suction, located 6mm below fingertip and with flow rate about 3L/min , which is based on our current design. Region C: suction is located 10mm below fingertip, with flow rate about 3L/min. Region D: 10mm below fingertip, 6L/min.) Results are mirrored for visual interpretation of grasp region.

where Q is the flow rate, r is a radial distance from the center of the orifice, and δ is the gap between the plates. Assuming inviscid flow and neglecting gravitational effects, Bernoulli's equation relates the pressure to the velocity:

$$\Delta P(r) = \frac{Q^2 \rho}{4\pi r \delta^2} \quad (9)$$

where ρ is fluid density. For overall suction force, assuming the stagnation zone is approximately the size of the orifice, we integrate the pressure over the fingertip:

$$F_s = \frac{Q^2 \rho}{4\pi \delta^2} \left(\ln \frac{W}{2} - \ln \frac{d}{2} \right) \quad (10)$$

where W is the width of the fingertip, assumed less than or equal to the object width, and d is the orifice diameter. Since water is viscous, the effective dimensions Q and δ will be somewhat reduced, however the trend that F_s increases with Q^2 and drops off with $1/\delta^2$ remains, as confirmed in Fig. 14 in Section V-A. The flat plate approximation is not valid for very small objects, but empirically the suction force will still tend to increase with Q and decrease as $1/\delta^2$.

B. Grasp Simulation with Suction

Simulations were run to determine the grasp region [25] for a neutrally-buoyant cylindrical object with various suction parameters. As shown in Fig. 11, grasp regions with and without suction were simulated based on empirical pump flow rate for various suction locations on the finger. To reduce the computation time, the finger was replaced with a model having constant joint stiffnesses and tendon moment arms that would produce a similar behavior (with larger required tendon forces). Since the suction position and flow rate of the current finger were chosen for small and slippery objects, they do not significantly improve the grasp region for a large cylinder with a diameter of 48 mm. However, by relocating the suction proximally a few millimeters, the region of acquisition increases (region C and D in Fig. 11). An interesting gap in the acquisition region is noted near $x = 12$ mm, $y = 0$ mm in which object attraction due to suction is not enough to prevent it from rolling out along the finger, resulting in grasp failure. These results demonstrate that changing the suction location and flow rate has the potential to significantly increase the acquisition region.

V. EXPERIMENTS AND RESULTS

Early experiments with the hand show that light suction is effective for acquiring and pinching small, slippery objects (see *video submission*). In addition, fingertip suction provides the ability to secure objects with just one finger. To test the strength of this effect and its dependence on object diameter, the hand was accelerated to various constant velocities using a robot arm to simulate an environmental disturbance flow around the finger and object; hand velocity at the 50% grasp failure rate was recorded. Figure 12 shows that small objects are strongly affected by suction, and that this effect is roughly proportional to flow rate. This result is expected because, as seen in Fig. 11, with the currently implemented fingertip suction, the grasp region for large objects is not increased.

A. Suction Model Verification

In order to verify the suction model described in Section IV, we measured the suction force on an object over a range

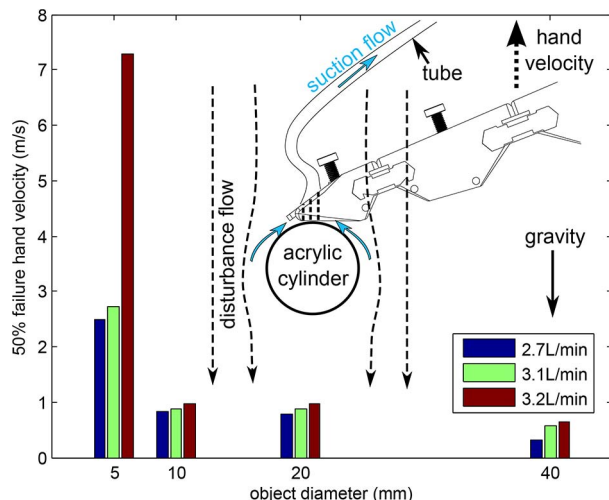


Fig. 12: Escape hand velocity for objects of various sizes (laminated acrylic cylinders 24mm wide and with varying diameters). Small objects are shown to be more susceptible to light suction at the fingertip.

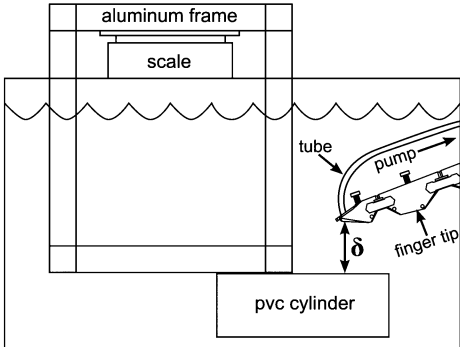


Fig. 13: Suction model testing setup.

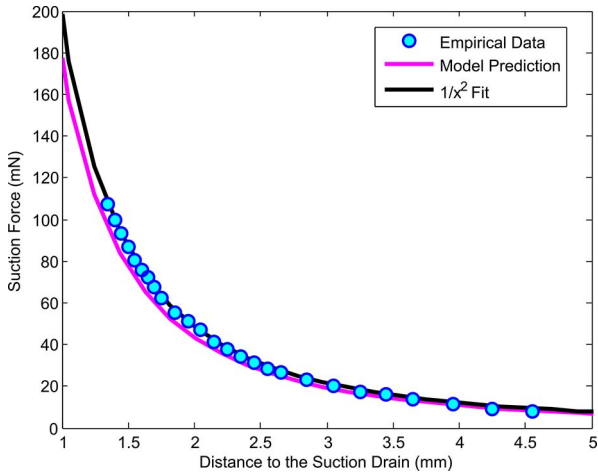


Fig. 14: Suction force for changing δ . The simplified flat plate model closely approximates the empirical data using estimated values of W and Q (eq. 10). An empirical $1/\delta^2$ fit to the data is used in grasp simulations.

of distances and compared this data with analytical and simulation results. A schematic of the setup, shown in Fig. 13, consists of a PVC cylinder, 48 mm in diameter, rigidly attached to an aluminum frame and suspended from a digital scale (force measurement accuracy of 0.001 N) such that the cylinder is fully submerged. The finger was oriented such that the flat face of the distal phalange was always parallel to the cylinder's tangent plane at the point of contact ($\delta = 0$). Suction was then applied to holes in the fingertip with a flow rate of 3.0 L/minute. As δ was varied, the scale measured the change in apparent weight of the frame-cylinder system upon the application of suction (i.e., the suction force).

As shown in Fig. 14, both the simplified flat plate model and the fitted model match the empirical data. Positioning resolution of the robot arm (0.001 mm) and the flexibility of the finger and test setup may account for experimental error.

B. Object Acquisition Region Testing

The planar underwater grasp region for a neutrally-buoyant plastic cylinder (48 mm diameter) was determined empirically. Figure 15 provides a schematic of the setup. The hand was attached to an Adept robot arm, used to translate the hand relative to the object. The object was positioned by attaching two magnets on the object to two low-stiffness ferromagnetic springs anchored to the bottom of a water-

filled tank. This suspension system was chosen to ensure consistent object positioning while also limiting its effects on the dynamics of grasping. Once the object and water settled, a grasp attempt was made by actuating all four fingers using individual motors at maximum velocity until stalled. The magnets detached as the hand contacted the object. Successful grasping was classified as four-fingered prismatic grasping (as in Fig. 1 (inset)). Ejection was classified as failure, and all other scenarios were disregarded.

Each location was tested three times. Figure 16 shows grasping results as compared to the grasp region predicted via simulation. There is clear agreement between empirical results and the simulated grasp envelope. The width of the experimental region is slightly larger than that of the simulation, likely due to the simplified geometry of the phalange models used in simulation.

VI. CONCLUSION

An underactuated hand is being developed for underwater mobile manipulation that uses compliant flexures, with a variable tendon and spring geometry to achieve a combination of pinch and wrap grasps without high tendon forces. The addition of gentle suction at the fingertips greatly improves the ability to acquire and grasp small and slippery objects underwater. Furthermore, modifying the suction location can improve the ability to acquire large objects.

A hand simulation that includes the effects of compliance, friction, drag and suction has been useful in evaluating different hand designs and establishing the region of object acquisition for each. Experiments with acquiring and grasping objects underwater confirm expected trends concerning the region of acquisition and the suction force.

VII. FUTURE WORK

The hand presented in this work is an initial prototype. The next version will be constructed from more durable polymers and will include tactile sensors and cast extension springs attached to features molded into the fingers. Suction will be integrated into the finger and, based on the simulation results in Fig. 11, an additional suction region will be located a few millimeters proximal to the current one. Future investigations will include surveying underwater grasp robustness through grasp trials with various objects, particularly as they

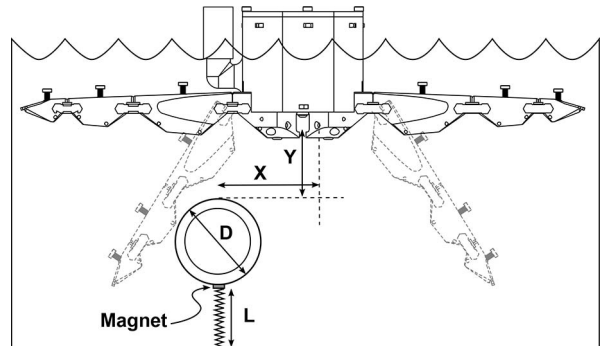


Fig. 15: Schematic of grasping experimental setup. X and Y define the coordinates of the center of the palm relative to the apex of the cylinder.

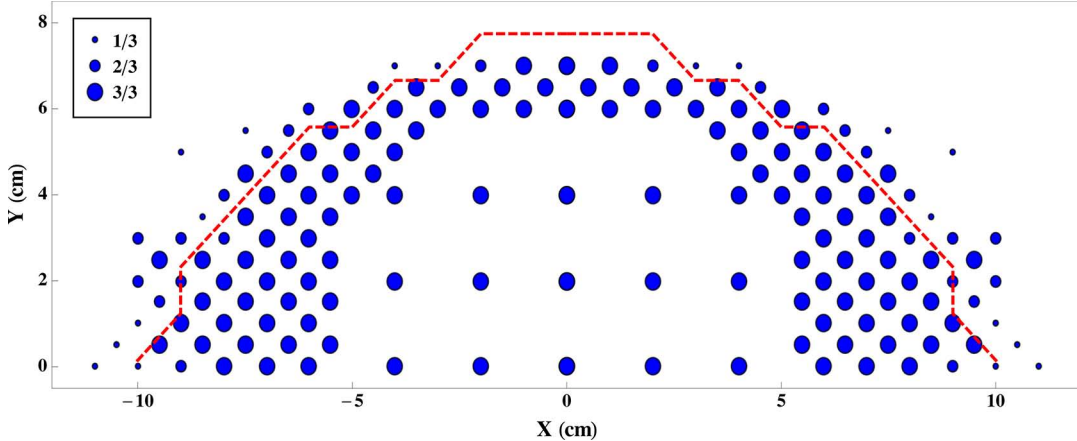


Fig. 16: Bubble chart depicting degrees of successful grasping without suction at various positions of the hand relative to the object. Three grasping trials were performed at each location tested. Larger circles indicate a greater number of successful trials. The red dotted line indicates the grasping envelope determined via simulation (also without suction).

change weight, rigidness, and surface friction. To improve the ability of our simulation to accurately model grasps of complex shapes, we also seek a deeper understanding of finger mechanics, including a more accurate model of three dimensional joint stiffness under general loading conditions.

An interesting future extension is to explore bimanual manipulation. It may be desirable for the left and right hands of the robot to be somewhat different, for example optimizing one for holding large objects securely and optimizing the other for working with small tools and grasping small and slippery objects.

ACKNOWLEDGMENT

This work has been supported by the KAUST Red Sea Robotics Research Exploratorium. H. Stuart and B. Gardner are additionally supported by NSF graduate fellowships. The assistance of Eduardo Moreno, Oussama Khatib, Torsten Kroeger, and Philip Mullins is gratefully acknowledged.

REFERENCES

- [1] A. M. Dollar and R. D. Howe, "Joint coupling design of underactuated hands for unstructured environments," *The International Journal of Robotics Research*, vol. 30, pp. 1157–1169, June 2011.
- [2] M. Catalano, G. Grioli, A. Serio, E. Farnioli, C. Piazza, and A. Bicchi, "Adaptive Synergies for a Humanoid Robot Hand," in *IEEE-RAS International Conference on Humanoid (In Press)*, (Osaka, Japan), 2012.
- [3] F. Lotti, P. Tiezzi, G. Vassura, L. Biagiotti, G. Palli, and C. Melchiorri, "Development of UB hand 3: Early results," in *2005 IEEE International Conference on Robotics and Automation*, pp. 4488–4493, 2005.
- [4] F. Ficuciello, G. Palli, and C. Melchiorri, "Experimental evaluation of Postural Synergies during Reach to Grasp with the UB Hand IV," *Intelligent Robots and*, pp. 1775–1780, 2011.
- [5] D. M. Aukes, S. Kim, P. Garcia, A. Edsinger, and M. R. Cutkosky, "Selectively compliant underactuated hand for mobile manipulation," in *2012 IEEE International Conference on Robotics and Automation*, pp. 2824–2829, IEEE, May 2012.
- [6] L. U. Odhner, R. R. Ma, and A. M. Dollar, "Open-Loop Precision Grasping With Underactuated Hands Inspired by a Human Manipulation Strategy," *IEEE Transactions on Automation Science and Engineering*, pp. 1–8, 2013.
- [7] M. Ciocarlie and P. Allen, "A constrained optimization framework for compliant underactuated grasping," *Mechanical Sciences*, vol. 2, pp. 17–26, Feb. 2011.
- [8] M. Carrozza, C. Suppo, F. Sebastiani, B. Massa, F. Vecchi, R. Lazarini, M. Cutkosky, and P. Dario, "The SPRING Hand: Development of a Self-Adaptive Prosthetic for Restoring Natural Grasping," *Autonomous Robots*, vol. 16, pp. 125–141, Mar. 2004.
- [9] D. M. Aukes, M. R. Cutkosky, S. Kim, J. Ulmen, P. Garcia, H. Stuart, and A. Edsinger, "Design and Testing of a Selectively Compliant Underactuated Hand," *International Journal of Robotics Research*(in press), 2013.
- [10] M. Cutkosky, "On grasp choice, grasp models, and the design of hands for manufacturing tasks," *IEEE Transactions on Robotics and Automation*, vol. 5, pp. 269–279, June 1989.
- [11] I. M. Bullock, J. Z. Zheng, S. De La Rosa, C. Guertler, and A. M. Dollar, "Grasp Frequency and Usage in Daily Household and Machine Shop Tasks," *IEEE Transactions on Haptics*(preprint), 2013.
- [12] L. Birglen, T. Laliberté, and C. Gosselin, *Underactuated Robotic Hands*, vol. 40 of *Springer Tracts in Advanced Robotics*. Berlin, Heidelberg: Springer Berlin Heidelberg, 2008.
- [13] D. M. Aukes, B. Heyneman, V. Duchaine, and M. R. Cutkosky, "Varying spring preloads to select grasp strategies in an adaptive hand," in *2011 IEEE/RSJ International Conference on Intelligent Robots and Systems*, pp. 1373–1379, IEEE, Sept. 2011.
- [14] Willow Garage, "2G "Velo" Gripper," 2013.
- [15] Robotiq, "3-Finger Adaptive Robot Gripper," 2013.
- [16] L. U. Odhner and A. M. Dollar, "The Smooth Curvature Model: An Efficient Representation of Euler–Bernoulli Flexures as Robot Joints," *IEEE Transactions on Robotics*, vol. 28, pp. 761–772, Aug. 2012.
- [17] L. Howell, *Compliant mechanisms*. Wiley-Interscience, 2001.
- [18] M. C. de Jong, J. A. Sparenberg, and J. de Vries, "Some aspects of the hydrodynamics of suction feeding of fish," *Fluid Dynamics Research*, vol. 2, pp. 87–112, Oct. 1987.
- [19] M. Muller, J. Osse, and J. Verhagen, "A quantitative hydrodynamical model of suction feeding in fish," *Journal of Theoretical Biology*, vol. 95, pp. 49–79, Mar. 1982.
- [20] F. Tramacere, L. Beccai, E. Sinibaldi, C. Laschi, and B. Mazzolai, "Adhesion Mechanisms Inspired by Octopus Suckers," *Procedia Computer Science*, vol. 7, pp. 192–193, Jan. 2011.
- [21] A. Dollar and R. Howe, "A robust compliant grasper via shape deposition manufacturing," *IEEE/ASME Transactions on Mechatronics*, vol. 11, no. 2, pp. 154–161, 2006.
- [22] E. Drumwright, "Moby Rigid Body Simulator."
- [23] J. D. Anderson, *Fundamentals of Aerodynamics*, vol. 1984. 1991.
- [24] M. Tachibana and Y. Iemoto, "Steady flow around, and drag on a circular cylinder moving at low speeds in a viscous liquid between two parallel planes," *Fluid dynamics research*, vol. 125, 1987.
- [25] R. Balasubramanian and A. M. Dollar, "A comparison of workspace and force capabilities between classes of underactuated mechanisms," in *2011 IEEE International Conference on Robotics and Automation*, pp. 3489–3496, IEEE, May 2011.